# NIH RELAIS Document Delivery

NIH-10286774

JEFFDUYN

NIH -- W1 MA34IF

JOZEF DUYN
10 Center Dirve
Bldg. 10/Rm.1L07
Bethesda, MD 20892-1150

ATTN:
PHONE: 301-594-7305
FAX: -
E-MAIL:

SUBMITTED: 2002-08-29 17:22:16
PRINTED: 2002-09-03 13:17:26
REQUEST NO.:NIH-10286774
SENT VIA: LOAN DOC
7967402

---

NIH Fiche to Paper Journal

---

TITLE: MAGNETIC RESONANCE IN MEDICINE : OFFICIAL JOURNAL OF THE SOCIETY OF MAGNETIC RESONANCE IN MEDICINE / SOCIETY OF MAGNETIC RESONANCE IN MEDICINE
PUBLISHER/PLACE: Wiley-Liss, Inc., a division of John Wil New York, NY :
VOLUME/ISSUE/PAGES:1998 Jan;39(1):61-7 61-7
DATE: 1998
AUTHOR OF ARTICLE: Yang Y; Glover GH; van Gelderen P; Patel AC; Mattay VS; Fran
TITLE OF ARTICLE: A comparison of fast MR scan techniques for cerebr
ISSN: 0740-3194
OTHER NOS/LETTERS: Library reports holding volume or year
8505245
9438438
SOURCE: PubMed
CALL NUMBER: W1 MA34IF
REQUESTER INFO: JEFFDUYN
DELIVERY: E-mail: jhd@helix.nih.gov
REPLY: Mail:

# A Comparison of Fast MR Scan Techniques for Cerebral Activation Studies at 1.5 Tesla

Yihong Yang, Gary H. Glover, Peter van Gelderen, Anand C. Patel, Venkata S. Mattay, Joseph A. Frank, Jeff H. Duyn

**To evaluate the sensitivity of fast, gradient-echo MR scan techniques in their ability to detect blood oxygenation level dependent (BOLD) signal changes in task activation studies, three dedicated fast scan techniques, each with whole-brain coverage, were compared during a 3-min finger tapping paradigm on nine normal volunteers on a clinical 1.5 T scanner. Multislice (2D) single-shot spiral, 3D spiral, and multislice (2D) single-shot EPI scan techniques were done with similar temporal and spatial resolutions on each of the volunteers in random order. After image registration and statistical analysis, the sensitivity to detect activation was evaluated for the techniques by calculating *t* scores and number of activated voxels in predetermined regions of interest, including the contralateral primary sensorimotor cortex, the premotor region, the parietal region, the supplementary motor area, and the ipsilateral cerebellum. Baseline images acquired with the three techniques were qualitatively comparable and had a similar effective spatial resolution of around $5 \times 5 \times 5$ mm$^3$, as determined from autocorrelation analysis. The anatomical coverage was somewhat reduced (4 less slices per volume) with EPI at the identical temporal resolution of 1.76 s for all techniques. The use of multislice 2D spiral scan for motor cortex fMRI experiments provided for a superior overall temporal stability, and an increased sensitivity compared with multislice 2D EPI, and 3D spiral scan. The difference in sensitivity between multislice 2D spiral and EPI scans was small, in particular in the case of a ramp-sampled version of EPI. The difference in performance is attributed mainly to the difference in scan-to-scan stability.**

**Key words: MRI; spiral scan; EPI; fMRI.**

## INTRODUCTION

Functional magnetic resonance imaging (fMRI) allows mapping of human brain function with the use of task activation studies, by employing a blood oxygenation level dependent (BOLD) image contrast (1). To detect the microscopic susceptibility effects related to changes in blood oxygenation with brain activity, a number of MR scan techniques have been used, including FLASH (2–4), echo planar imaging (EPI) (5–8), spiral scan (9–13), and hybrids (14, 15).

**MRM 39:61–67 (1998)**

From the Laboratory of Diagnostic Radiology Research, OIR, (Y.Y., A.C.P., J.A.F., J.H.D.), In Vivo NMR Research Center, BEIP, NCRR (P.v.G.), Clinical Brain Disorders Branch, NIMH (V.S.M.), National Institutes of Health, Bethesda, Maryland; and the Department of Diagnostic Radiology, Lucas MRI Center, Stanford University School of Medicine, Stanford, California (G.H.G.).

Address correspondence to: Jeff H. Duyn, Ph.D., Laboratory of Diagnostic Radiology Research, OIR, National Institutes of Health, Building 10, Room BIN-256, Bethesda, MD 20892.

Received January 29, 1997; revised June 12, 1997 accepted June 16, 1997.

0740-3194/98 $3.00



An important issue in the evaluation of fMRI scan techniques is the sensitivity for detection of activated regions, which can be defined as the activation-related increase in image intensity divided by the standard deviation of the signal time course. The former is dependent on experimental parameters such as echo time (*TE*) of the scan, whereas the latter is determined by signal fluctuations caused by subject motion, physiological pulsations, and electronic scanner noise. A poor sensitivity requires increased signal averaging to improve statistical power (e.g., *t* score) for detection of activation, leading to lengthening of the fMRI experiment. In general, faster MR scan methods, such as EPI and spiral scan, allow for reduction of the relative contribution of instabilities resulting from subject motion and cardiac and respiratory cycles, resulting in improved sensitivity and therefore shorter study times.

With the recent improvements in gradient hardware on clinical scanners, one can expect an increase in the use of EPI and spiral imaging. These techniques are now able to cover the entire brain within scan times in the order of 2–6 s, either in a multislice acquisition mode, or in a true 3D fashion (8, 13). Although multislice EPI has been and still is the most popular fMRI acquisition technique, so far no studies have been presented comparing its value with either spiral scan or 3D acquisition techniques. In this study, both image quality and sensitivity of EPI and spiral fMRI scan methods are compared in motor cortex activation experiments on normal volunteers.

## MATERIALS AND METHODS

All studies were performed as part of a protocol at the National Institutes of Health and were approved by the Intramural Research Board. MR scanning was done on a 1.5 Tesla GE-SIGNA scanner (General Electric, Milwaukee, WI), running an EPIC 5.5 platform, equipped with an insertable gradient/RF coil assembly (Medical Advances, Milwaukee, WI) with maximum gradient strength of 22 mT.m$^{-1}$ and maximum slew rate of 210 T.m$^{-1}$.s$^{-1}$ on all three axes. The comparisons were perfomed on the insert coil, to avoid the restrictive limitations on amplifier duty cycle of the current gradient system. The insert coil was not run at its maximum slew rate, but at a maximum of 120 T.m$^{-1}$.s$^{-1}$ instead, to stay within the specifications of the standard (whole body) gradients.

### Spiral Scanning

The spiral scan technique was run in two different modalities: as a multislice single-shot 2D experiment and in a true 3D fashion. In both cases, axial sections (slices) through the brain were scanned. Spiral waveforms of 22

ms duration were applied in two orthogonal directions for in-plane imaging. The waveforms were designed for minimum time of acquisition (TACQ) at a given resolution, by using a slew rate limited (120 $T.m^{-1}.s^{-1}$) design, with a maximum gradient amplitude of 20 $mT.m^{-1}$. A nominal in-plane resolution of 3.75 × 3.75 $mm^2$ was achieved with a single repetition of the pulse sequence. The multislice version excited 36 axial slices (4 mm thick each) in two sequential interleaves (1-3-5-. . . and 2-4-6. . . ). For the 3D experiment, a slab of 130-mm thickness in the z (longitudinal) direction was selected using an optimized Shinnar-Le Roux selective excitation pulse (16), and a 36-step phase encoding cycle was applied in the z direction. The field of view (FOV) in the z direction was set to 144 mm to render a 4-mm nominal slice thickness. The choice of a slightly larger FOV compared with the slab thickness was made to avoid aliasing effects resulting from imperfect slab profiles. The scan-to-scan stability was optimized by gradient moment nulling of the slice select gradient (13) as well as the use of a quadratic RF phase modulation scheme with a periodicity of eight (17).

### EPI Scanning

The EPI scan was performed as a multislice 2D experiment, with close similarities to the multislice 2D spiral version. In essence, the only difference between the techniques were the gradient waveforms for imaging (readout and phase encode). To optimize the EPI sequence, imaging gradients were designed with minimum duration of 41 ms. This included 20 ms of gradient ramping (including 5 ms of blipped gradient), and resulted in an effective data acquisition duration of 21 ms, which was similar to the spiral scans (22 ms).

### Task Activation Studies

To choose optimum *TE* for the activation studies, five data sets (with different *TE*s) were acquired on each subject (three subjects totally) using the multislice spiral and EPI sequences. *TE*/*TR* values were set at 20/39, 35/54, 50/69, 65/84, and 80/99 ms for the spiral scan, and 25/50, 35/60, 50/75, 65/90, 80/115 ms for the EPI scan (*TE* of 20 ms in the EPI was not allowed). For each *TE*/*TR* setting, the flip angle was adjusted to match the Ernst angle (assuming $T_1$ = 800 ms for gray matter). Each data set was acquired in 3 min with a alternative finger tapping paradigm (see below).

For comparison of the three scan techniques, BOLD functional imaging with sensorimotor cortex activation was performed on nine normal subjects, using each of the three scan techniques. The order of acquisition for the techniques was randomized, as to minimize systematic bias among the experiments. The echo time (*TE*), as counted from the center of the RF excitation pulse to the center of the data acquisition window, was identical (30 ms) for all three pulse sequences. This resulted in similar image intensity changes with activation across the three experiments. This relatively low value of *TE* (relative to previously suggested optimum values around the $T_2$* of gray matter, i.e., 70 ms (18)) was chosen to permit a short repetition time (*TR*), resulting in reduced sensitivity to motion (12, 13), and an increase in the number of whole brain scans per unit time, as well as to provide good sensitivity in areas with poor background shimming (e.g., lower brain areas). Consequently, the shortest *TR* value was chosen for each technique (49 ms for both spiral techniques, and 55 ms for EPI). To keep an identical time resolution (1.76 s per volume) for all studies, the number of slices was reduced to 32 (from 36) in the EPI experiments. To optimize the signal-to-noise ratio (SNR) for gray matter in each technique, the RF flip angle (FA) was set at the Ernst angle (84° for multislice 2D spiral and EPI, and 20° for 3D spiral, assuming $T_1$ = 800 ms for gray matter). In each functional study, a time series of 102 scans was acquired in 3 min, during which the subject switched between rest and finger tapping every 30 s (3 "off-states" and 3 "on-states"). The finger tapping was self-paced (2 Hz) and consisted of sequential thumb-to-digit oppositions (in the order of 2, 3, 4, 5, 5, 4, 3, 2) with the dominant hand. The subjects were supplied with ear plugs due to the high levels of acoustic noise during scanning, and foam packs were applied to restrict head motion.

### Data Processing

Data were processed off line on Sun-SPARC (Sun Microsystems, Mountain View, CA) and SGI-Indigo (Silicon Graphics, Mountain View, CA) workstations. The signal processing language IDL (Research Systems, Boulder, CO) was used for most of the data processing, except the reconstruction of the spiral images and registration. The latter processing steps were performed using a custom-written software package.

For the 3D spiral data, an initial 1D Fourier transform was performed in the phase-encode direction (longitudinal direction) with cosine apodization. Subsequently, for both 2D and 3D spiral data, a regridding algorithm with a Gaussian convolution window was used to re-sample the data on an orthogonal equidistant grid on transverse plane (19). The regridding included corrections for zeroth and first order off-resonance effects, calculated from separately recorded $B_0$ maps (20). For the EPI data, off-resonance corrections were performed with the use of reference data acquired with one of the localization gradients ("blipped gradients") switched off (21). For all techniques, before Fourier transformations in the two axial directions in the transverse plane, the data was apodized by a radial cosine filter. The effective in-plane resolution, calculated from the area of the simulated 2D point-spread function (PSF) at half of its peak magnitude, was 1.96 $pixel^2$ (equivalent to 1.40 pixels width of rectangular PSF). This value does not include broadening caused by image artifacts, such as off-resonance effects. Therefore, the actual image resolution was estimated from the functional data by computing the full width at half maximum (FWHM) of the spatial autocorrelation function for each of the techniques (22–24). This estimate assumed a Gaussian noise distribution within the images.

All images were registered to the last image to correct for rigid body motion between scans. The registration routine was based on a custom written software package,

using a multiresolution least squares difference algorithm with cubic spline interpolation (25, 26). The functional data were analyzed by means of a $t$ test in predefined region-of-interest (ROI), adjusted for total number of voxels in the ROI by a Bonferroni correction. For each subject, a ROI was defined covering the contralateral primary sensorimotor cortex, the premotor region, the parietal region, the supplementary motor area, and the ipsilateral cerebellum (8). The total number of voxels in the ROI was typically 420, resulting in a Bonferroni corrected significance threshold of $P < 5.95 \times 10^{-5}$ (0.025/420) per voxel. The corresponding $t$ cutoff was approximately 4.0, and voxels with $t$ score above the threshold were considered as significantly activated. The total number of activated voxels and the average $t$ score of the activated voxels in the ROI were calculated for each subject.

To evaluate the scan-to-scan stability of the techniques, the standard deviation of the image intensity over acquisition time was calculated for each voxel in the brain and presented as a histogram. This measure of signal stability included effects of tissue motion/pulsation, as well as scanner noise.

### Simulations

Computer simulations were performed to simulate the image point-spread function (PSF) for the following purposes:

1. To calculate the effect of circular versus rectangular apodization windows applied to the EPI data on the image resolution.
2. To estimate the effect of acquisition time (TACQ) on the $T_2$* weighting for both spiral scan and EPI.

The image resolution was calculated from the surface area at half height of the PSF. The linear (1D) resolution was then determined by taking the square root of this area. The effect of TACQ on the $T_2$* weighting was determined by calculating the $k$-space representation of a uniform object, and determine the distortions introduced by local alterations in $T_2$*. The effective $TE$ was then calculated from the local shift in image intensity in the center of the area with altered $T_2$*, as a function of its diameter.

## RESULTS

### Image Quality

The images of the multislice and 3D spiral techniques, as well as multislice EPI were qualitatively similar. Figure 1 shows two subsets of brain images acquired with the multislice spiral and EPI sequences. The phase correction used in image reconstruction was effective in most of the brain, although blurring (spiral) and warping (EPI) appeared in the orbito-frontal regions at the air-tissue interface and the regions of the mastoid sinus. The average effective image resolution, estimated from the FWHM of the spatial autocorrelation function for the multislice spiral and EPI, and 3D spiral are shown in Table 1. In-plane resolutions were similar among the three scan techniques. Longitudinal resolutions in the multislice spiral and EPI scan techniques were similar, but were around 10% better than the 3D scan technique (due to the longitudinal apodization in the 3D technique).

### *TE* Dependence

Figure 2 shows the signal increases, number of activated voxels, and average $t$ score within the activated motor cortex as a function of $TE$, for the multislice spiral and EPI experiments. BOLD signal changes increased with $TE$ due to stronger $T_2$* weighting (top diagram), although at the cost of an increase in temporal standard deviation (not shown). The overall sensitivity for detection of activated regions (reflected by the number of activated voxels and average $t$ score, shown in the middle and bottom

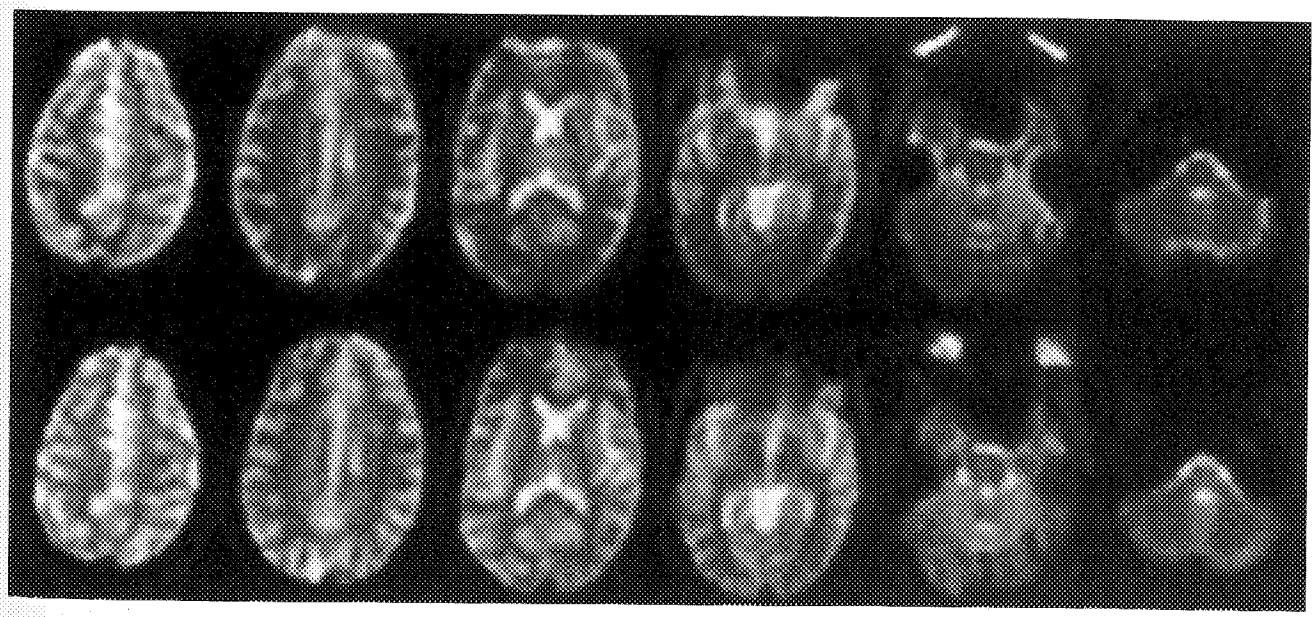

FIG. 1. Subsets of brain images acquired with the single-shot spiral (top row) and EPI (bottom row) sequences, respectively. Displayed is the first data set of a time series. Later time points showed reduced image contrast, due to saturation effects.

Table 1
Effective Spatial Resolution Estimated by the FWHM of the Spatial Autocorrelation Function for the Multislice Spiral and EPI, and 3D Spiral Techniques

| | Effective in-plane (*x-y*) resolution (in pixels) | Effective through-plane (*z*) resolution (in pixels) |
|---|---|---|
| MS spiral | 1.44 ± 0.05 | 1.14 ± 0.04 |
| MS EPI | 1.47 ± 0.05 | 1.15 ± 0.07 |
| 3D spiral | 1.45 ± 0.04 | 1.25 ± 0.06 |

diagram) was fairly flat in the *TE* range of 30–70 ms (within 84% of the maximum number of activated voxels, and 93% of the maximum average *t* score), attributed to the improved temporal stability and increased number of scans per unit time, for the studies with shorter *TE*'s.

## Temporal Stability

The standard deviation was normalized to the baseline voxel intensity. With all three imaging techniques, the distribution was fairly uniform across the brain. Increased standard deviation values were typically found in the area surrounding the posterior fossa, and at air-tissue interfaces. The lower intensity for the multislice spiral data suggests a better scan-to-scan stability.

For each of the techniques, the distribution of standard deviation values in voxels across the brain was summarized in a histogram. A comparison of composite histograms including all subjects for multislice spiral, 3D spiral, and multislice EPI is shown in Fig. 3. The peak positions of the histograms are $7.9 \times 10^{-3}$ for multislice spiral, $9.8 \times 10^{-3}$ for multislice EPI, and $9.7 \times 10^{-3}$ for 3D spiral. Paired Student *t* test showed that the peak position of the standard deviation distribution in the multislice spiral was significantly lower than that in the multislice EPI ($P < 0.001$) and in the 3D spiral ($P < 0.002$). The FWHM of the distribution curve was $0.32 \times 10^{-3}$ in the multislice spiral, $0.34 \times 10^{-3}$ in the multislice EPI, and $0.35 \times 10^{-3}$ in the 3D spiral. There was no significant difference in the FWHM among the three sequences.

## Overall Sensitivity

A comparison of activation maps in the motor cortex region, obtained with each of the three scan techniques, is shown in Fig. 4. Clearly visible is activation in the contralateral primary sensorimotor cortex, the premotor region, the parietal region, the supplementary motor area, and the ipsilateral cerebellum. Similar activation maps were observed in all subjects, although the cerebella activation was not shown in two of the nine subjects (for all three techniques).

A more accurate assessment of the sensitivity can be made from the number of activated voxels within the preselected ROI, together with the average *t* score of the activated voxels. Figure 5 shows composite histograms of the ROI-based *t* score from all subjects, for each of the three sequences. Each curve represents activated as well as nonactivated voxels within each ROI. The vertical line at $t = 4.0$ represents the imposed separation between activated and nonactivated voxels. Comparison of the curves right of this cut-off suggest a higher number of activated voxels with the multislice spiral as compared

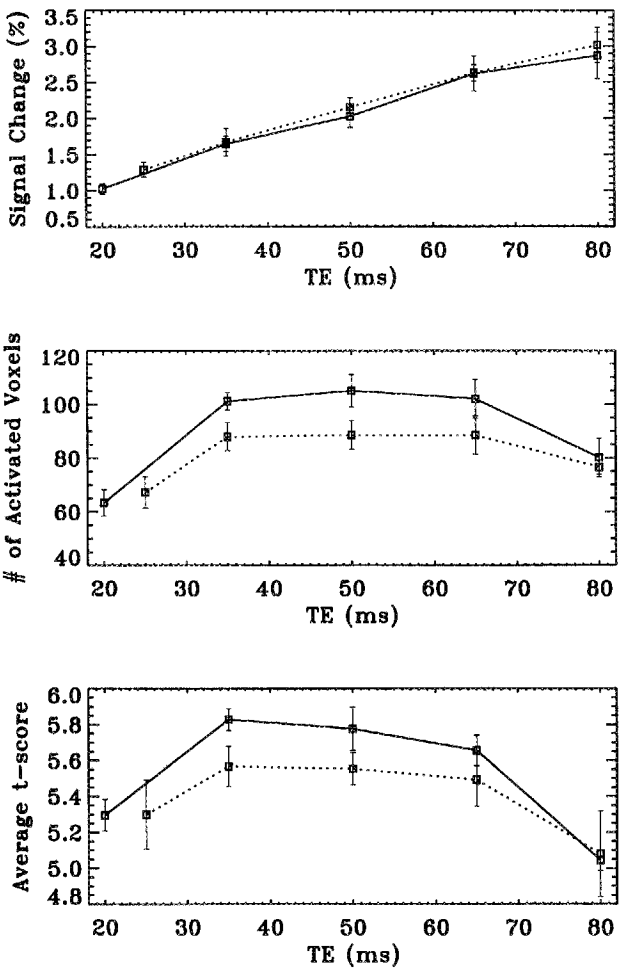


FIG. 2. Averaged signal increases (top), number of activated voxels (middle), and average *t* score (bottom) in the activated motor cortex as a function of echo time in the multislice spiral (solid lines) and EPI (dotted lines) scans.

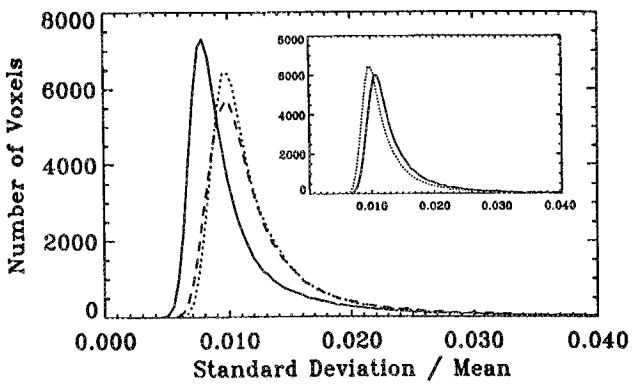


FIG. 3. Histograms of standard deviations of the image intensity time course for all voxels in the brains, and summed over all subjects. The three curves represent the multislice spiral (solid line), the multislice EPI (dotted line), and the 3D spiral (dashed line) scans. The insert shows the histograms of standard deviations for EPI with circular filter (dotted line) and square filter (solid line).

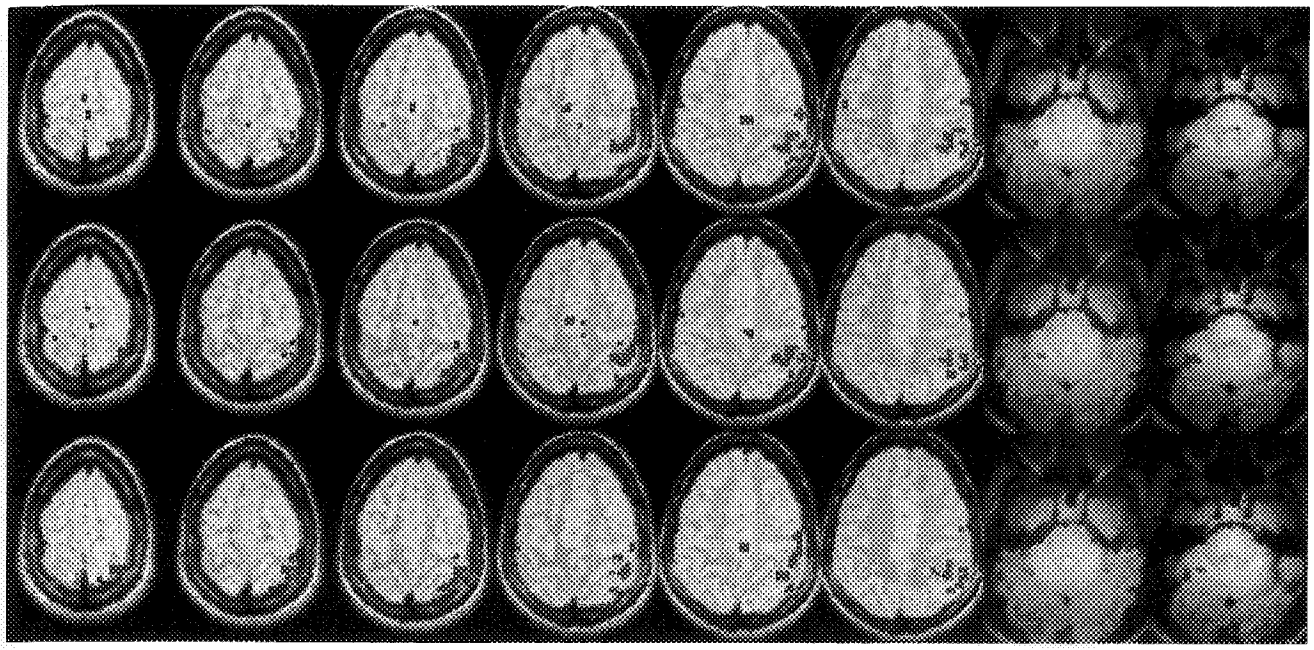

FIG. 4. An example of sensorimotor activation maps obtained from the multislice spiral (top row), multislice EPI (middle row), and 3D spiral studies (bottom row). The voxels with significant activation (see text) are displayed in red, and overlaid on corresponding $T_2$-weighted images.

with the multislice EPI, as well as to the 3D spiral. The total number of voxels above the threshold were 814, 673, and 679, respectively, and the average $t$ score of these voxels were 5.67, 5.50, and 5.52 for all ROIs. The data for the individual subject is summarized in Table 2. Paired Student $t$ tests showed that the number of activated voxels in the multislice spiral was significantly higher than that in the multislice EPI ($P < 0.002$) and in the 3D spiral ($P < 0.004$). The average $t$ score of the activated voxels in the multislice spiral was also significantly higher than that in the multislice EPI ($P < 0.01$) and in the 3D spiral ($P < 0.006$). There were no significant differences in the number of activated voxels and average $t$ score between the multislice EPI and 3D spiral sequences.

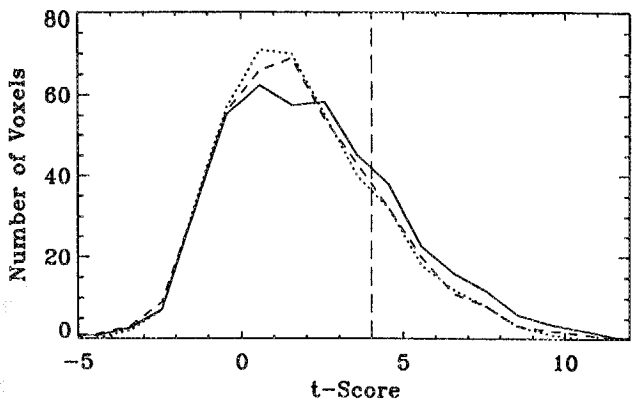


FIG. 5. Composite histograms of the $t$ scores for the voxels in all ROIs of all subjects. The three curves correspond to the multislice spiral (solid line), the multislice EPI (dotted line), and the 3D spiral (dashed line) sequences, respectively. Voxels with a $t$ score above 4.0 (cutoff indicated with vertical line) were considered activated.

Signal increases due to brain activation were calculated within the ROIs for the activated voxels shared between three techniques. The signal changes were 1.38 ± 0.29%, 1.48 ± 0.27%, and 1.42 ± 0.25% for the multislice spiral, multislice EPI, and 3D spiral, respectively.

## DISCUSSION

### Effective Spatial Resolution

The average actual resolution in the functional images, as determined from the autocorrelation analysis, followed the theoretical predictions from analysis of the point-spread function (PSF). This suggests that the effect of artifacts (e.g., blurring) on the resolution was relatively small in most of the brain. One note has to be made with respect to the use of apodization filters in this study. The relative loss in resolution caused by the circular filter is relatively higher for the EPI data, which is acquired in a rectangular $k$-space format. The circular filter was chosen to obtain comparable resolution for all techniques. The use of a square filter for EPI data resulted in a 13% narrower PSF, although at the cost of some SNR, as determined by simulation. Experimental data showed that the square filter caused a 10 ± 1% increase in temporal standard deviation of the image intensity (i.e., a loss in stability), as compared with that with the circular filter (Fig. 3). This suggests that one could modify the EPI acquisition to match the PSF width of the spiral scan, and reduce the bandwidth (e.g., by performing circular EPI (27)). This would increase the SNR by around 13%, and could lead to a small overall improvement in stability. In addition, the use of ramp sampling in EPI allows reduction of the bandwidth, which slightly improves the stability for EPI scans. Comparison of non-ramp-sampled

Table 2
Number of Activated Voxels and Average *t* Scores of the Voxels, Summed over all ROIs

| Volunteer | Number of activated voxels | | | Average *t* score | | |
|---|---|---|---|---|---|---|
| | MS spiral | MS EPI | 3D spiral | MS spiral | MS EPI | 3D spiral |
| 1 | 87 | 72 | 70 | 5.66 | 5.53 | 5.50 |
| 2 | 112 | 88 | 80 | 6.02 | 5.88 | 5.76 |
| 3 | 96 | 65 | 76 | 5.62 | 5.22 | 5.55 |
| 4 | 75 | 77 | 76 | 5.49 | 5.53 | 5.47 |
| 5 | 88 | 78 | 75 | 5.70 | 5.61 | 5.52 |
| 6 | 68 | 48 | 47 | 5.52 | 5.20 | 5.36 |
| 7 | 86 | 88 | 82 | 5.22 | 5.23 | 5.27 |
| 8 | 104 | 80 | 91 | 6.04 | 5.85 | 5.90 |
| 9 | 98 | 77 | 82 | 5.52 | 5.30 | 5.22 |
| Mean | 90.4 | 74.8 | 75.4 | 5.64 | 5.48 | 5.50 |
| SD | 13.8 | 12.3 | 12.2 | 0.26 | 0.26 | 0.22 |

versus ramp-sampled EPI versions showed a 10% stability improvement for the latter.

### Overall Sensitivity

The activation related relative signal changes are expected to be similar for all three techniques, because of the uniform *TE* value of 30 ms. This assumes comparable image tissue contrast and comparable $T_2$* weighting for the three techniques. In this situation, the overall sensitivity is determined by the scan-to-scan stability, which can be estimated from temporal standard deviation (Fig. 3).

The superior stability of multislice spiral compared with EPI under comparable conditions is partly attributed to their different sensitivities to motion and flow artifacts. This relates to the fundamental differences in *k*-space trajectories. Spiral trajectories have excellent flow properties, including zero gradient moments at the origin of *k*-space, and smoothly varying first order gradient moments over *k*-space (10, 28). Earlier results from simulation analysis demonstrated that spiral images were almost immune to flow artifacts up to linear velocities of 20 cm/s, while EPI images showed intensity distortions and ghosting (28). Vascular spins, for example, are therefore more likely to cause signal instabilities in EPI than in spiral MRI.

The stability difference between multislice and 3D scanning (Fig. 3) stems from the differences in data acquisition. In the multislice mode, data acquisition was independent for each slice, resulting in a relatively short acquisition time (equivalent to TACQ, i.e., 22 ms for spiral scan). For the 3D experiment, all slices are acquired "simultaneously," with the acquisition time (for each slice) stretching out over the duration for acquiring entire volume (1.76 s in this study). Therefore, signal fluctuations on this time scale (related to cardiac and respiratory cycles, and CSF pulsations) more severely affect 3D data. A potential improvement in the 3D experiment is the use of navigator echoes to correct for some of these motion-induced signal fluctuations. In addition, in situations where the overall *TR* (scan time per volume) is much larger than the tissue $T_1$, the SNR advantage of 3D scanning possibly becomes an issue.

### Effective Echo Time

The amount of BOLD-related signal expected with activation is dependent on the $T_2$* weighting, which depends on the delay between RF excitation and data acquisition (*TE*). Due to significant duration of TACQ, *TE* is ill-defined with spiral and EPI scans. In addition, the $T_2$*-related signal decay during TACQ affects the PSF (i.e., resolution), and results in shifting of intensity in the images. The actual $T_2$* related signal loss within one voxel, and consequently the signal increase with activation, is therefore dependent on *k*-space trajectory, spatial apodization, and size of the activated area. The $T_2$* weighting of a technique is therefore more appropriately indicated by the "effective *TE*," or *TE**. With spiral techniques, *TE** is close to the center of acquisition window for the smallest (sub-voxel size) activated regions, but shifts toward the start of acquisition window for larger regions (Fig. 6). For clusters with a diameter (in the axial plane) of more than three pixel dimensions, *TE** is closer to the start of acquisition window. On the other hand, for EPI, *TE** is close to the center of acquisition window for any cluster size. Based on these considerations, the relative signal change with activation is expected to be somewhat larger with EPI than that with spiral scan. This is in agreement with the experiments, which showed a 6% larger signal change with activation with EPI (see Results).

In the spiral scan technique, a potential increase in signal change with activation can be achieved by reversing the spiral waveforms (i.e., a spiral-in acquisition (29)). This substantially increases *TE** for all but the smallest clusters. However, it does not guarantee an increase in overall sensitivity. Under the current conditions, the temporal standard deviation was increased around 45% with spiral-in acquisition, resulting in a

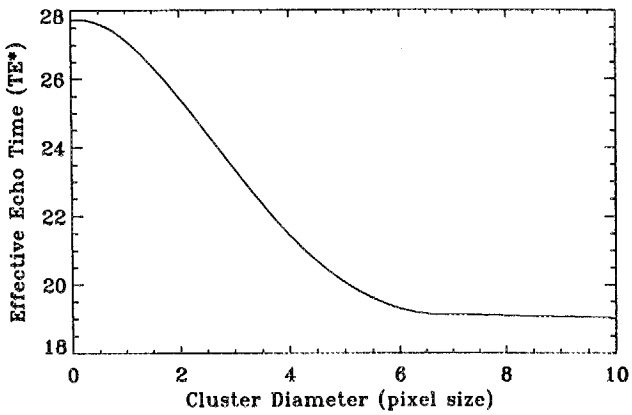


FIG. 6. Calculated effective $T_2$* weighting (*TE**) as a function of cluster diameter for spiral acquisition (parameters corresponding to experimental conditions described in Methods). Note that for small cluster diameters, the *TE** is close to the center of the acquisition window, whereas for cluster diameters of three or more voxels, *TE** approaches the start of the acquisition window (center of *k*-space).

sensitivity increase only for the larger clusters (>3 pixels diameter).

### Computational Requirements

Although the reconstruction time for the spiral data was substantially longer than that for EPI (25 min versus 7 min on an SGI-Indigo Workstation using C-code), it did not dramatically lengthen the total duration of the fMRI analysis. This was because of the extensive computational requirements of the image registration, which took up most of the (1.5 h) processing time. Therefore, the spiral reconstruction time did not lead to a severe limitation with regard to the duration of the image analysis.

## CONCLUSION

The use of multislice 2D spiral scan for motor cortex fMRI experiments provided for a superior overall temporal stability, and an increased sensitivity compared with multislice 2D EPI, and 3D spiral scan. The difference in sensitivity between 2D spiral scan and 2D EPI was small, in particular in the case of a ramp-sampled version of EPI.

## ACKNOWLEDGMENTS

The authors thank Dr. Marcus Alley (Standard University) for providing an SLR-optimized RF slice selection waveform, Dr. Attanagoda K. S. Santha (National Institutes of Health) for technical support regarding the fMRI analysis, and Mr. Kenneth C. Schalk (University of Illinois at Urbana-Champaign) for providing a 3D matrix library for $C^{++}$ programming of the spiral reconstruction software.

## REFERENCES

1. S. Ogawa, T. M. Lee, A. R. Ray, D. W. Tank, Brain magnetic resonance imaging with contrast dependent on blood oxygenation. *Proc. Natl. Acad. Sci. USA* **87,** 9868–9872 (1990).
2. S. Ogawa, D. W. Tank, R. Menon, J. M. Ellerman, S. Kim, H. Merkle, K. Ugurbil, Intrinsic signal changes accompanying sensory stimulation: functional brain mapping using MRI. *Proc. Natl. Acad. Sci. USA* **89,** 5951–5955 (1992).
3. J. Frahm, H. Bruhn, K. Merboldt, W. Hänicke, Dynamic MR imaging of human brain oxygenation during rest and photic stimulation. *J. Magn. Reson. Imaging* **2,** 501–505 (1992).
4. S. G. Kim, J. Ashe, A. P. Georgopoulos, H. Merkle, J. M. Ellermann, R. S. Menon, S. Ogawa, K. Ugurbil, Functional imaging of human motor cortex at high magnetic field. *J. Neurophysiol.* **69,** 297–302 (1993).
5. P. Mansfield, I. Pykett, Biological and medical imaging by NMR. *J. Magn. Reson.* **29,** 355–373 (1978).
6. K. K. Kwong, J. W. Belliveau, D. A. Chesler, I. E. Goldberg, R. M. Weiskoff, B. P. Poncelet, D. N. Kennedy, B. E. Hoppel, M. S. Cohen, R. Turner, H. Cheng, T. J. Brady, B. R. Rosen, Dynamic magnetic resonance imaging of human brain activity during primary sensory stimulation. *Proc. Natl. Acad. Sci. USA* **89,** 5675–5679 (1992).
7. P. A. Bandettini, E. C. Wong, R. S. Hinks, R. S. Tikofsky, J. S. Hyde, Time course EPI of human brain function during task activation. *Magn. Reson. Med.* **25,** 390–397 (1992).
8. V. S. Mattay, J. A. Frank, A. K. S. Santha, J. J. Pekar, J. H. Duyn, A. C. McLaughlin, D. R. Weinberger, Whole-brain functional mapping with isotropic MR imaging. *Radiology* **201,** 399–404 (1996).
9. R. S. Likes, Moving gradient zeugmatography. U.S. Patent 4307343 (1981).
10. C. H. Meyer, B. S. Hu, D. G. Nishimura, A. Macovski, Fast spiral coronary artery imaging. *Magn. Reson. Med.* **28,** 202–213 (1992).
11. D. C. Noll, J. D. Cohen, Meyer C. H. Meyer, W. Schneider, Spiral k-space MR imaging of cortical activation. *J. Magn. Reson. Imaging* **5,** 49–56 (1995).
12. G. H. Glover, A. T. Lee, Motion artifacts in fMRI: comparison of 2DFT with PR and spiral scan methods. *Magn. Reson. Med.* **33,** 624–635 (1995).
13. Y. Yang, G. H. Glover, P. van Gelderen, V. S. Mattay, A. K. S. Santha, R. H. Sexton, N. F. Ramsey, C. T. W. Moonen, D. R. Weinberger, J. A. Frank, J. H. Duyn, Fast 3D functional magnetic resonance imaging at 1.5 T with spiral acquisition. *Magn. Reson. Med.* **36,** 620–626 (1996).
14. C. M. J. van Uijen, J. H. den Boef, F. J. J. Verschuren, Fast Fourier imaging. *Magn. Reson. Med.* **2,** 203–217 (1985).
15. P. van Gelderen, N. F. Ramsey, G. Liu, J. H. Duyn, J. A. Frank, D. R. Weinberger, C. T. W. Moonen, Three-dimensional functional magnetic resonance imaging of human brain on a clinical 1.5-T scanner. *Proc. Natl. Acad. Sci. USA* **92,** 6906–6910 (1995).
16. J. M. Pauly, P. Le Roux, D. G. Nishimura, A. Macovski, Parameter relations for the Shinnar-Le Roux selective excitation pulse design algorithm. *IEEE Trans. Med. Imaging* **10,** 53–65 (1991).
17. J. H. Duyn, Steady state effects in fast gradient echo imaging. *Magn. Reson. Med.* **37,** 559–568 (1997).
18. R. S. Menon, S. Ogawa, D. W. Tank, Ugurbil K, 4 Tesla gradient recalled echo characteristics of photic stimulation-induced signal changes in the human primary visual cortex. *Magn. Reson. Med.* **30,** 380–386 (1993).
19. J. I. Jackson, C. H. Meyer, D. G. Nishimura, A. Macovski, Selection of a convolution function for Fourier inversion using gridding. *IEEE Trans. Med. Imaging* **10,** 473–478 (1991).
20. E. Yudilevich, H. Stark, Spiral sampling in magnetic resonance imaging: the effect of inhomogeneities. *IEEE Trans. Med. Imaging* **6,** 337–345 (1987).
21. E. C. Wong, Shim insensitive phase correction for EPI using a two echo reference scan, *in* "Proc., SMRM, 11th Annual Meeting, Berlin, 1992," p. 4514.
22. K. J. Friston, P. Jezzard, R. Turner, Analysis of fMRI time-series. *Hum. Brain Mapping* **1,** 153–171 (1994).
23. K. J. Worsley, K. J. Friston, Analysis of fMRI time-series revisited—again. *Neuroimaging* **2,** 173–181 (1995).
24. J. Xiong, J. H. Gao, J. L. Lancaster, P. Fox, Clustered pixel analysis for functional MRI activation studies of the human brain. *Hum. Brain Mapping* **3,** 287–301 (1995).
25. M. Unser, A. Aldroubi, A multiresolution image registration procedure using spline pyramids, *in* "Proc., SPIE, San Diego, 1993, vol. 2034, Mathematical Imaging: Wavelet Applications in Signal and Image Processing," pp. 160–170.
26. P. Thevenaz, U. E. Ruttimann, M. Unser, Iterative multi-scale registration without landmarks, *in* "Proc., International Conference on Image Processing, Washington, D.C., 1995, vol. 3," pp. 228–231.
27. J. M. Pauly, K. Butts, G. T. Luk-Pat, A. Macovski, A circular echo-planar pulse sequence, *in* "Proc., SMR, 3rd Annual Meeting, Nice, France, 1995," p.106.
28. D. G. Nishimura, P. Irarrazabal, C. H. Meyer, A velocity k-space analysis of flow effects in echo-plannar and spiral imaging. *Magn. Reson. Med.* **33,** 549–556 (1995).
29. C. H. Mayer, K. C. P. Li, J. M. Pauly, A. Macovski, Fast spiral T 2-weighted imaging, *in* "Proc., SMRM, 13th Annual Meeting, San Francisco, 1994," p.467.